

***Listeria monocytogenes* induces host DNA damage and delays the host cell cycle to promote infection**

Elsa Leitão¹, Ana Catarina Costa¹, Cláudia Brito, Lionel Costa, Rita Pombinho, Didier Cabanes*, Sandra Sousa*

Group of Molecular Microbiology, Infection and Immunity, IBMC – Instituto de Biologia Molecular e Celular, Universidade do Porto, 4150-180 Porto, Portugal

¹ These authors contributed equally to this work.

Contact Information

*srsousa@ibmc.up.pt or didier@ibmc.up.pt

Tel.: +351226074900, Fax: +351226099157

Running title *Listeria* delays host cell cycle to favor infection

Keywords: Bacterial infection, *Listeria monocytogenes*, Host cell cycle, DNA damage, DNA-PK, Cdc25A

ABSTRACT

Listeria monocytogenes (*Lm*) is a human intracellular pathogen widely used to uncover the mechanisms evolved by pathogens to establish infection. However its capacity to perturb the host cell cycle was never reported. We show that *Lm* infection affects the host cell cycle progression increasing its overall duration but allowing consecutive rounds of division. A complete *Lm* infectious cycle induces a S-phase delay accompanied by a slower rate of DNA synthesis and increased levels of host DNA strand breaks. Additionally, DNA damage/replication checkpoint responses are triggered in an *Lm* dose-dependent manner through the phosphorylation of DNA-PK, H2AX and CDC25A and independently from ATM/ATR. While host DNA damage induced exogenously favors *Lm* dissemination, the override of checkpoint pathways limits infection. We propose that host DNA replication disturbed by *Lm* infection culminates in DNA strand breaks, triggering DNA damage/replication responses and ensuring a cell cycle delay that favors *Lm* propagation.

INTRODUCTION

Listeria monocytogenes (*Lm*) is a facultative intracellular foodborne pathogen able to cross human tight barriers and spread from cell to cell causing listeriosis, a severe human disease.¹ *Lm* employs an arsenal of virulence factors to invade, survive and multiply in both phagocytic and non-phagocytic cells,² hijacking host signaling pathways to establish and sustain infection.³

Several bacterial pathogens were shown to modulate the host cell cycle to support infection. Bacterial effectors such as cyclomodulins^{4,5} can inhibit or stimulate the eukaryotic cell cycle, playing roles in disease. While *Shigella* and pathogenic *Escherichia coli* block host cells in the G2/M phase transition,⁶⁻⁸ *Neisseria gonorrhoeae* and *Porphyromonas gingivalis* inhibit cell proliferation via G1 arrest.^{9,10} Conversely, *Helicobacter pylori* enhances gastric epithelial cell proliferation by stimulating cell cycle progression.¹¹ In addition, *H. pylori* was reported to induce host DNA double strand breaks contributing to genetic instability and chromosomal aberrations typical of gastric cancer.¹² *Chlamydia trachomatis* was epidemiologically linked to increased risk of developing cervical cancer.¹³ It affects genome stability by several mechanisms: multipolar spindle formation,^{14,15} spindle assembly checkpoint override,¹⁶ cytokinesis failure^{17,18} and induction of DNA damage coupled to impaired repair mechanisms.¹⁹

The interplay between *Lm* and the host cell cycle is understudied. Albeit *Lm* remains mostly cytosolic, it interferes with histone modifications^{20,21} and chromatin regulatory factors²² to modulate host gene expression.

As pathogens often exploit similar pathways to cause infection, we investigated if *Lm* interferes with the host cell cycle progression to create a suitable replication niche.

RESULTS

***Lm*-infected cells show increased cell cycle duration**

To investigate if *Listeria*-infected cells were able to undergo complete and consecutive division cycles, we performed live-cell imaging of Caco-2 cells infected for 72h with GFP-expressing *Lm* (hereafter *Lm*). Phase contrast images were acquired at 10 min intervals, and *Lm* infection was confirmed by acquisition of intracellular GFP signal every 40 min (Movie S1). Analysis of independent movies showed that infected cells divide and undergo successive division cycles (Movie S2). Figure 1A shows consecutive cell division steps of an infected cell giving rise to two infected daughter cells. We observed that *Lm* is excluded from the mitotic spindle during mitosis (Figure 1B) as previously described,²³ and that both daughter cells inherited a comparable number of bacteria (Figure 1A).

The cell cycle duration of uninfected (NI) and *Lm*-infected (Inf) cells was determined by measuring the time elapsed between consecutive metaphase plates. The cell cycle duration was 3.5 h longer in Inf (23.8 ± 0.7 h) as compared to NI cells (20.3 ± 0.4 h) (Figure 1C). Importantly, infection did not affect cell viability for at least 40 h (Figure 1D). Together these data indicate that *Lm* infection does not prevent host cell division but modulates cell cycle progression.

***Lm* infection alters the host cell cycle phase distribution**

The *Lm*-induced increase in the host cell cycle duration prompted us to compare cell cycle phase distribution profiles of infected and uninfected (NI) cells. Unsynchronized Caco-2 and Jeg-3 cells were left NI or *Lm*-infected for 17 h (Inf). Flow cytometry analysis of unfixed cells showed that viability was not affected by infection (Figure S1A). In Caco-2 cells we detected 75% of infected and 25% of uninfected bystander cells (Figure S1B), while 57% of Jeg-3 cells were infected (data not shown). Flow cytometry DNA histograms were generated from three cell subsets: NI, cells containing intracellular bacteria (Inf GFP+) and uninfected bystander cells (Inf GFP-). The Inf

GFP+ Caco-2 subset revealed a significant and consistent increase of cells in S- and G2/M-phases, and a concomitant decrease in G1/G0, as compared to NI and Inf GFP- cell populations (Figure 2A). Importantly, NI and bystander Inf GFP- cells showed comparable cell cycle phase distributions. Similar results were observed in Jeg-3 cells (Figure 2A).

Since the majority of cells in *Lm*-incubated flasks have intracellular bacteria, we assessed if the effect of *Lm* infection was still detectable in the mixed population (GFP+ and GFP- cells). Compared to NI cells, DNA histograms obtained for Inf Caco-2 cells also revealed an increase of cells in S- and G2/M-phases and a decrease in G1/G0 (Figure 2B). Similarly, Inf Jeg-3 cells showed a slight but consistent accumulation of S-phase and a reduction in G1/G0 (Figure 2B). Moreover, in Caco-2 cells, these cell cycle phase distribution changes were *Lm* dose-dependent (Figure 2C). These effects were still observed in mixed populations with only 33% of Inf cells (Figure S2). Sub-G1 peaks corresponding to hypodiploid or apoptotic cells were undetectable (Figure 2A, 2B). These data indicate that *Lm* induces dose-dependent cell cycle alterations in different cell lines, which require the presence of intracellular bacteria but are independent on cellular or *Lm*-secreted factors acting from the extracellular milieu.

Host cell cycle alterations require a complete *Lm* cellular infection cycle

To evaluate the role of well-known bacterial factors in the alterations on the host cell cycle phase distribution, we performed infections with several engineered bacterial strains. Cells were left uninfected (NI) or infected with *Lm* or *L. innocua* expressing InIA (*Li*-InIA), a strain that mimics *Lm* invasion of Caco-2 cells but cannot escape from the phagocytic vacuole and replicate in the host cytoplasm. We used a 100-fold higher multiplicity of infection (MOI) for *Li*-InIA to obtain similar percentages of infected cells 17 h post-infection (77% for *Lm* and 70% for *Li*-InIA). However, colony-forming unit (CFU) counting showed 10-fold less intracellular *Li*-InIA than *Lm*. The analysis of mixed

populations (Figure 2D) and discriminated Inf GFP⁺ and Inf GFP⁻ cells (Figure S3) revealed that NI and *Li*-InIA-infected cells have similar percentage of cells in S- and G2/M-phases. A slight decrease in G1/G0 cell fraction was detected only after mixed population analysis of *Li*-InIA-infected cells (Figure 2D). These results suggest that cellular invasion is not sufficient to induce alterations of the host cell cycle profile.

To corroborate these data, Jeg-3 cells, in which *Lm* entry is driven by both InIA and InIB invasins, were kept NI or infected with *Lm* Δ *inIA*, *Lm* Δ *inIB* or *Lm* Δ *inIAB* mutants and DNA histograms were obtained from Inf GFP⁺ and Inf GFP⁻ cells. As found for *Lm* infection, while cell cycle profiles were similar for Inf GFP⁻ and NI cells, differences in S- and/or G1/G0-phases were detected in *Lm* Δ *inIA*- and *Lm* Δ *inIB*-infected cells (Figure 2E). As expected *Lm* Δ *inIAB* infected very few cells, inducing only slight but not statistically significant differences in S- and/or G1/G0-phase cell fractions (Figure 2E). These results indicate that *Lm* entry, and InIA- and InIB-activated signaling are not sufficient to induce cell cycle stage alterations. In addition, Caco-2 cells infected by *Lm* Δ *hly*, a strain that invades cells but is impaired in vacuolar escape displayed a cell cycle profile in-between NI and *Lm*-infected cells (Figure 2F), suggesting that the pore-forming toxin listeriolysin O (LLO, encoded by *hly*) might be partially responsible but not sufficient to induce host cell cycle alterations.

Together these data show that *Lm* interference with the host cell cycle distribution does not fully depend on any of the major virulence factors tested, and that a complete *Lm* cellular infection cycle appears required to cause host cell cycle alterations.

Albeit the analysis of mixed cell populations underestimates the effects, considering our data and technical issues, we pursued analyzing the effects of *Lm* infection on mixed populations of Caco-2 cells, comprising mainly infected cells.

***Lm*-infected cells are delayed in S-phase**

The accumulation of cells in S-phase suggested that *Lm* could be delaying the progression through this phase. To verify this, Caco-2 cells synchronized at the G1/S-

phase boundary were simultaneously infected and released from the cell cycle arrest and DNA histograms of NI and Inf cells were analyzed 5 h later. While both histograms had perfectly superimposable G1 peaks, a leftwards shift was detected in the S-phase curve of Inf cells, indicating a slightly delayed S-phase (Figure 3A). Analysis of split S-phase statistics showed that, while the proportion of Inf relative to NI cells is higher in early S-phase (S1/S2) it is lower in late S-phase stages (S3/S4) (Figure 3B), suggesting again that Inf cells progress slower in S-phase. To strengthen our data, we analyzed the progression of cells in S-phase by measuring the percentage of EdU (an analog of thymidine incorporated in DNA during synthesis) positive cells. Unsynchronized NI or Inf Caco-2 cells were incubated with EdU and analyzed immediately or after a 5 h chase. Inf cells showed higher percentage of S-phase cells and lower levels of EdU incorporation (EdU+ mean fluorescence intensity, MFI), confirming that *Lm* infection slows S-phase progression and correlating the accumulation of S-phase cells with slower DNA synthesis (Figure 3C, D, E). Five hours after EdU washout we still detected a higher percentage of Inf cells in S-phase. Consequently, the subsequent G1/G0 cells were barely detected in infection conditions whereas clearly present in NI cells (red arrow, EdU+) (Figure 3F, G). A slightly decreased G2/M cell fraction was also observed in Inf samples (data not shown). Our data show that *Lm* disturbs the rate of DNA synthesis inducing an S-phase delay, which should account for the host cell cycle profile alterations and the increased cell cycle duration.

***Lm* infection induces host cell DNA injury**

Given that DNA integrity controls the progression through S-phase, we evaluated this parameter in NI and Inf Caco-2 cells. We measured single and double strand breaks (SSBs and DSBs) in individualized cells by single-cell gel electrophoresis (SCGE). Inf cells showed a higher percentage of comet tail intensity as compared to NI cells (Figure 4A), indicating that they suffer more DNA strand breaks. As expected, the DNA

damage inducers etoposide (Etop) and γ -irradiation (IR) caused higher tail intensity percentages. To corroborate these results we performed pulse-field gel electrophoresis (PFGE) to visualize intact and fragmented DNA. Bands corresponding to fragmented DNA were faint in NI samples and more intense in Inf, Etop and IR cells, reflecting a higher amount of undersized chromosomal DNA molecules (Figure 4B). Using different amounts of *Lm* we showed that *Lm* genomic DNA was undetectable even in highly concentrated samples (Figure S4), thus ruling out the possibility that *Lm* genomic DNA could account for the presence of bands corresponding to fragmented DNA in Inf cells. Host DNA injury was also monitored through the levels of histone H2A.X phosphorylation (γ H2A.X), a hallmark of DNA damage. Immunoblot assays showed that levels of γ H2A.X, normalized to total H2A.X, were augmented by 50% and 70% in *Lm*- and *Lm* Δ *hly*-infected cells, respectively (Figure 4C). As for the accumulation of cells in S-phase, *Lm* triggers a dose-dependent γ H2A.X increase (Figure 4D). In addition, immunofluorescence analysis showed a 2-fold increase in the number and intensity of γ H2A.X foci in Inf as compared to NI cells (Figure 4E). Altogether these data show that *Lm* infection induces host DNA strand breaks, an event that appears independent of LLO.

DNA damage checkpoint override impairs *Lm* infection

Given that *Lm* induces host DNA strand breaks, we hypothesized that it could trigger DNA damage checkpoint responses and that the effects on the host cell cycle would come from a physiological response to DNA injury. We conducted infection assays in the presence or absence of caffeine, a widely used pleiotropic inhibitor of DNA damage checkpoint responses,²⁴ and generated DNA histograms. Caffeine prevented the effect of *Lm* infection on the host cell cycle as shown by the similar cell cycle profiles of Inf and NI cells (Figure 5A). Caffeine-induced override of DNA damage checkpoints was confirmed by the abrogation of the γ -irradiation effects (IR). These data suggest that

Lm infection affects the host cell cycle progression *via* DNA damage checkpoint responses.

To verify if the increased cell cycle duration of Inf cells was due to checkpoint responses, we quantified the cell cycle duration of NI and Inf cells in the presence or absence of caffeine. We found that caffeine abrogated the increase in cell cycle duration detected in Inf cells as compared to NI cells (Figure 5B). Caffeine-induced augmentation of cell cycle duration was previously reported.²⁵ These data suggest that host cell cycle delay is related to the *Lm* ability to cause host DNA injury and the consequent engagement of checkpoint responses.

We then investigated the role of DNA damage checkpoints in *Lm* infection. We found that the override of DNA damage checkpoints by caffeine leads to a 20% decrease in the number of Inf GFP+ cells and a 40% decrease of GFP+ MFI, suggesting the presence of fewer intracellular *Lm* (Figure 5C, 5D). In agreement, CFU counting showed that caffeine decreased the number of intracellular bacteria to about 40%, as compared to untreated cells (Figure 5D). We verified that caffeine had no effect on *Lm* growth in pure culture (Figure S5). To confirm that DNA damage and checkpoints activation favors *Lm* infection, we infected Caco-2 cells treated with increasing doses of etoposide and evaluated the *Lm* infectious potential. We found that etoposide induced a dose-dependent increase of both the percentage of GFP+ cells and their MFI, indicating that *Lm*-infection is favored in DNA-damaged cells (Figure 5E, F).

Altogether, our results demonstrate that the *Lm* ability to induce host DNA damage and activate checkpoint responses creates an advantageous dissemination niche.

***Lm*-induced effects on host cell cycle require DNA-PK**

Lm ability to induce host DNA damage and activate DNA damage responses led us to investigate the role of central kinases in this context, namely ATM and ATR, damage sensors and enforcers of checkpoint activation; and DNA-PK, a key regulator of DSB repair. We analyzed DNA histograms of Caco-2 cells treated with control (siCtr),

ATM/ATR (siATM/ATR)- or DNA-PK (siDNA-PK)-specific siRNAs, in uninfected (NI) and *Lm*-infected (Inf) conditions. Cell cycle distribution profiles of siCtr or siATM/ATR Inf cells showed increased S- and decreased G1/G0-phase cell fractions, as compared to NI cells (Figure 6A). In DNA-PK-depleted Inf cells, only slight but not statistically significant changes were detected in S- and G1/G0-phases as compared to NI cells, indicating that DNA-PK depletion abrogated the effects of *Lm* infection on the host cell cycle (Figure 6A). In agreement, while similar percentages of Inf GFP+ cells and GFP+ MFI were detected in siATM/ATR and siCtr cells, DNA-PK depletion decreased the percentage of infected cells and the number of intracellular bacteria (Figure 6B), as observed in caffeine-treated cells (Figure 5C, D). In siRNA-treated cells, ATM and ATR expression levels fell by 75%, whereas DNA-PK levels decreased only by 25% (Figure 6C). Altogether these results indicate that *Lm* induces host cell cycle profile alterations in a DNA-PK-dependent manner and independently of ATM and ATR. In addition, our data suggest that DNA damage/repair pathways driven by DNA-PK support *Lm* infection.

***Lm* elicits DNA damage/repair mechanisms via DNA-PK and CDC25A**

To further investigate the role of DNA-PK in *Lm* infection we monitored its phosphorylation, which is involved in DSB sensing and repair.²⁶ Caco-2 cells were infected with increasing MOIs (0.1-1) or treated with increasing doses of etoposide (0.1-40 μ M), and analyzed by immunoblot. Levels of phosphorylated DNA-PK (p-DNA-PK) increased in a dose-dependent manner in response to increasing MOIs and etoposide doses (Figure 7A). As shown in Figure 4D, γ H2A.X levels, which can be regulated by DNA-PK,^{27,28} followed a similar trend (Figure 7A). Interestingly, using a cell cycle antibody array (FullMoon BiosystemsTM) to identify proteins differentially phosphorylated in response to *Lm* infection, we found a 2.5-fold increase in phosphorylated CDC25A levels (data not shown), a key phosphatase in DNA damage checkpoint responses and cell cycle regulation, particularly in S-phase.²⁹ Given that

CDC25A is phosphorylated in response to DNA damage, preventing cell cycle progression to allow DNA repair,²⁹ we corroborated the array results by immunoblot, confirming that phosphorylated CDC25A levels (p-CDC25A) increased upon infection and etoposide treatment (Figure 7A). According to the results of dose-response experiments we consider that the outcome of *Lm* infection (MOI=0.5, 17 h) corresponds to the genotoxic effect induced by 0.1-1 μ M etoposide. Altogether these results suggest that *Lm* triggers DNA damage/repair signaling that possibly leads to S-phase delay.

To assess if *Lm*-induced DNA damage and downstream signaling occur during *in vivo* infection, immunoblots were performed using total cell extracts from spleens of *Lm*-infected (Inf) and uninfected (NI) mice. While cell viability was similar in NI and *Lm*-infected spleens (Figure S6), increased levels of γ H2A.X were detected in spleen cells from mice infected for 1 and 3 days (Figure 7B, C), strongly suggesting that DNA damage is occurring in infected mice organs. In addition, CDC25A was phosphorylated in spleen cells from 3-day infected mice (Figure 7C) showing the *in vivo* engagement of host DNA damage/repair mechanisms.

DISCUSSION

The interplay between *Lm* and the host cell nucleus has only been addressed from an epigenetic viewpoint. Here, we evaluated if *Lm* interferes with the host cell cycle to create a suitable colonization niche. We showed that *Lm* infection hinders the host cell cycle progression increasing its duration without compromising cell division and viability. *Lm*-infected cells have a slower rate of DNA synthesis accumulating in S-phase and showing increased DNA strand breaks. Host cell cycle delay favors *Lm* infection and relies on DNA damage/replication checkpoint responses triggered by DNA-PK activation.

We showed for the first time in live cells that *Lm*-infected cells divide giving rise to infected daughter cells. Contrarily to other pathogens causing cell cycle arrest, *Lm* produces a mild phenotype that allows complete cell division yet adjusting cell cycle to its own benefit. This can provide a dual advantage for *Lm*, favoring dissemination of the infection and enabling the control of its intracellular numbers to avoid cell damage. Albeit achieving cell division, different infected cell lines showed a consistent and dose-dependent accumulation in S-phase that is not driven by bacterial adhesion or entry and is independent of any cellular or bacterial secreted factors acting from the extracellular milieu. The crosstalk between *Lm* and the host cell cycle should occur when *Lm* is free in the cytosol and thus depends on a complete *Lm* infection cycle.

Besides the S-phase delay, we also detected an increase in G2/M and a decrease in G1/G0 population. These effects deserve further studies to unravel if they result from a direct action of *Lm* or are a consequence of the S-phase hindrance.

The consistently slower progression of *Lm*-infected cells through S-phase lead us to propose that *Lm* could perturb host DNA replication, which can be disturbed by DNA damage, DNA-bound proteins, aberrant DNA structures and nucleotide starvation.³⁰ Free in the host cytosol *Lm* acquires nutrients from the host and multiplies as in rich medium,³¹ rerouting resources available for the host metabolism. In particular, *Lm*

could be competing for dNTPs, whose pools are tightly regulated to preserve genome integrity.³⁰ Indeed, continued DNA synthesis in conditions of low dNTP shortage leads to reduced replication rates and increased DNA breaks,³² events that we observed in infected cells. In turn, as host cell proliferation is a highly demanding process, the *Lm*-induced cell cycle delay could offer bacteria extra nutrients favoring its own growth.

Another hypothesis relies in the capacity of several bacterial pathogens to trigger histone modifications modulating host transcription through epigenetic features.³³ *Lm* modifies host gene expression *via* two virulence factors, LntA and LLO.^{20-22,34} LLO modulates host transcription from the extracellular milieu and is degraded once *Lm* escapes the vacuole, being unlikely to modify host histones from the cytoplasm.²⁰ Our data do not support a crucial role for LLO or any other bacterial secreted proteins acting from the extracellular milieu. Nevertheless, it is plausible that pathogen-induced DNA damage results from the crosstalk between host transcription modulation and DNA replication, where cellular machineries would compete for the access to DNA. Indeed, stalled replication forks may become unstable and prone to collapse, thus activating DNA damage/replication responses.³⁰ Our data indicate that *Lm* infection elicits DNA damage/replication responses, which delay cell cycle progression to allow possible DNA repair and/or fork protection.

Besides *Lm*, other bacterial pathogens have been shown to cause host DNA strand breaks. Producers of genotoxins such as cytolethal distending toxins or colibactin, cause direct DNA injury inducing genomic instability and ultimately cell cycle arrest and cell death.^{7,35-37} Other bacteria, such as *C. trachomatis*,¹⁹ *Pseudomonas aeruginosa*,³⁸ *H. pylori*,¹² *N. gonorrhoeae*³⁹ and *Shigella flexneri*,⁴⁰ induce the production of reactive oxygen species (ROS) that promote oxidative DNA damage, thereby increasing γ H2A.X levels and impairing host DNA repair mechanisms. To our knowledge, *Lm* does not express toxins that can directly injure host DNA. In addition, *Lm* was described to inhibit ROS through the action of LLO,⁴¹ suggesting a new bacterial mechanism to induce host DNA injury.

Lm-induced DNA damage responses are independent from ATM and ATR, the major DNA damage sensors, indicating that *Lm* infection does not engage the canonical DNA damage response, as described for other pathogens.¹² *Lm* signals *via* another DNA damage sensor and key repair enzyme, DNA-PK. Upon infection, DNA-PK is phosphorylated in an *Lm* dose-dependent manner, together with H2AX and CDC25A. γ H2AX is a central factor in the crossroad of several DNA damage/repair pathways, responding to multiple sensors and targeting various effectors. CDC25A regulates early and late cell cycle transitions and is phosphorylated in response to DNA damage or stalled replication inducing an S-phase delay and preventing the cell cycle progression of damaged cells.

Several pathogens that interfere with the host cell cycle cause persistent infections, inducing host cell genomic instability, impairing DNA repair and promoting tumor development.^{5,42} *Lm* was never associated with enhanced risk in cancer development and persistent *Lm* infections are yet poorly supported. However, wild type *Lm* and highly attenuated mutants were found to persist in small foci in the mouse bone marrow.⁴³ Importantly, attenuated *Lm* strains have been used as a delivery system in anti-cancer therapies⁴⁴ and considered serious candidates for anti-cancer vaccines^{45,46}. Our data are particularly important in this context, as we show that *Lm* causes DNA damage in diverse host cells possibly contributing to genomic instability. Additionally, *Lm* infection is potentiated in environments where host DNA is already injured. Our study opens new perspectives to uncover the long-term effects of *Lm* infection.

Although other scenarios can be put forward, we propose that *Lm* proliferation in the host cytoplasm interferes with host DNA replication, culminating in fork arrest and DNA strand breaks. Infected cells would sense this damage and trigger DNA damage/replication checkpoint responses *via* DNA-PK, ensuring a cell cycle progression delay that allows DNA repair and/or replication fork protection. Such delay would also insure a favorable environment for *Lm* replication, possibly through an increase in resource availability.

EXPERIMENTAL PROCEDURES

Infection assays

Caco-2 or Jeg-3 cells were seeded at 6×10^5 cells per 60-mm dish (Nunc) and propagated for 48 h. Bacteria were grown to an OD_{600} of 0.7, washed and diluted in EMEM. Cells were incubated with *Lm* at MOI 0.1-1, *Lm* Δ *hly* at MOI 10, *Lm* Δ *inIA*, *Lm* Δ *inIB*, or *Lm* Δ *inIAB* at MOI 0.1, or *Li*-*InIA* at MOI 50. After 1 h of invasion cells were kept for 16-19 h in complete medium supplemented with 50 μ g/ml gentamicin, plus 2 mM caffeine or 0.1-10 μ M etoposide. Intracellular bacteria were quantified as described.⁴⁷ Synchronized cells infections are detailed in Supplemental Experimental Procedures.

Flow cytometry analyses

To assess cell viability and quantify infected cells, unfixed cells were resuspended in PBS with 2% FBS and 2.5 μ g/ml propidium iodide (PI). Percentage of infected cells (%GFP+) and their mean GFP fluorescence intensity (GFP+ MFI) were evaluated on a GFP-A/PE-A plot, after exclusion of debris, cell doublets and dead cells. To generate DNA histograms, cells were fixed in 70% ethanol and incubated (37°C, 3 h) with 40 μ g/ml PI and 10 μ g/ml RNase A. Alternatively, to avoid GFP signal quenching, cells were fixed using a combined paraformaldehyde (PFA)/ethanol method. Single-cell suspensions were fixed (1 h, 4°C) in Cytfix (BD Biosciences) and 70% ethanol (30 min) and incubated with PI and RNaseA. At least 10 000 gated events were acquired in a FACS Canto II flow cytometer (BD Biosciences). DNA histograms were obtained on a linear-scale PE-A histogram, after exclusion of debris and cell doublets. In PFA/ethanol-fixed samples, GFP+ (infected) and GFP- (bystander) populations were discriminated. Data were analyzed using FlowJo software (TreeStar, Inc.) and the Watson pragmatic model to quantify the percentage of cells per phase. Whenever stated, split S-phase statistics were performed, allowing the division of S-phase Gaussian curve in four populations with equally spaced peaks (S1-4).

Click-iT EdU Flow Cytometry Assay Kit (Invitrogen) was used to label cells in S-phase. Infected (16 h) and uninfected Caco-2 cells were incubated for 2 h with 20 μ M Click-iT EdU. To evaluate S-phase exit, EdU was washed out and cells allowed to progress for 5 h. The percentage of EdU+ cells was analyzed by flow cytometry on an APC/PE contour plot.

Time-lapse microscopy

Caco-2 cells seeded at 2×10^4 cells per Ibitreat μ -dishes (Ibidi) were grown for 24 h and left uninfected or infected with *Lm* at MOI 0.1. After 1 h of invasion, cells were cultured in gentamicin-supplemented phenol red-free medium, plus caffeine (whenever stated), and followed for 72 h by live-cell imaging. Images were acquired in an inverted epifluorescence Axiovert 200M microscope (Zeiss) equipped with a NanoScan Piezo Z stage (Prior Scientific Instruments). Cells were maintained at 37°C in a 7% CO₂ humidified atmosphere. Shutters, filter wheels and point visiting were driven by Micro-Manager 1.4 software⁴⁸ and images captured with a CoolSNAP HQ camera (Roper Scientific). Phase contrast images were acquired every 10 min and GFP signal images every 40 min, at multiple points with a 20x (0.30 NA) objective. Fiji software was used to compile images, merge phase contrast with GFP signal and analyze the resulting movies.

Please refer to Supplemental Experimental Procedures for details concerning: bacterial strains, cell lines and growth conditions, SCGE, PFGE, immunoblot and immunofluorescence analyses, siRNA transfection and mice experiments.

Statistical analyses

Statistical analyses were performed with Prism 6 software (GraphPad Software, Inc.). One-way ANOVA with post hoc testing analyses were used for pair-wise comparison of means from three or more unmatched groups. Two-tailed Student's t-test was used to

compare means of two samples and one-sample t-test to compare with samples arbitrarily fixed to 100. Differences were not considered statistically significant for p value ≥ 0.05 .

ACKNOWLEDGMENTS

We thank AFCU and ALM facilities (IBMC), T. Duarte (IBMC), G. Almeida and R. Guimarães (ESB) for technical support, M. Moroso for the *LmΔin/B* strain and members of Maiato's and Sunkel's lab (IBMC) for fruitful discussions. This work was funded by FCT, COMPETE and FEDER programs (PTDC/BIA-BCM/111215/2009FCOMP-01-0124-FEDER-014178, ERANet-Pathogenomics LISTRESS ERA-PTG/0003/2010). EL, ACC and RP were supported by FCT grants (SFRH/BPD/62926/2009, SFRH/BPD/88769/2012 and SFRH/BD/89542/2012, respectively), LC by ERASMUS program and SS by Ciência 2008 program (COMPETE, POPH and FCT).

REFERENCES

1. Swaminathan B, Gerner-Smidt P. The epidemiology of human listeriosis. *Microbes Infect* 2007; 9:1236-43.
2. Camejo A, Carvalho F, Reis O, Leitao E, Sousa S, Cabanes D. The arsenal of virulence factors deployed by *Listeria monocytogenes* to promote its cell infection cycle. *Virulence* 2011; 2:379-94.
3. Pizarro-Cerda J, Kuhbacher A, Cossart P. Entry of *Listeria monocytogenes* in mammalian epithelial cells: An updated view. *Cold Spring Harb Perspect Med* 2012; 2.
4. Nougayrede JP, Taieb F, De Rycke J, Oswald E. Cyclomodulins: bacterial effectors that modulate the eukaryotic cell cycle. *Trends Microbiol* 2005; 13:103-10.
5. Oswald E, Nougayrede JP, Taieb F, Sugai M. Bacterial toxins that modulate host cell-cycle progression. *Curr Opin Microbiol* 2005; 8:83-91.
6. Iwai H, Kim M, Yoshikawa Y, Ashida H, Ogawa M, Fujita Y, Muller D, Kirikae T, Jackson PK, Kotani S, et al. A bacterial effector targets Mad2L2, an APC inhibitor, to modulate host cell cycling. *Cell* 2007; 130:611-23.
7. Nougayrede JP, Homburg S, Taieb F, Boury M, Brzuszkiewicz E, Gottschalk G, Buchrieser C, Hacker J, Dobrindt U, Oswald E. *Escherichia coli* induces DNA double-strand breaks in eukaryotic cells. *Science* 2006; 313:848-51.
8. Taieb F, Nougayrede JP, Watrin C, Samba-Louaka A, Oswald E. *Escherichia coli* cyclomodulin Cif induces G₂ arrest of the host cell cycle without activation of the DNA-damage checkpoint-signalling pathway. *Cell Microbiol* 2006; 8:1910-21.
9. Inaba H, Kuboniwa M, Bainbridge B, Yilmaz O, Katz J, Shiverick KT, Amano A, Lamont RJ. *Porphyromonas gingivalis* invades human trophoblasts and inhibits proliferation by inducing G1 arrest and apoptosis. *Cell Microbiol* 2009; 11:1517-32.
10. Jones A, Jonsson AB, Aro H. *Neisseria gonorrhoeae* infection causes a G1 arrest in human epithelial cells. *FASEB J* 2007; 21:345-55.

11. Peek RM, Blaser MJ, Mays DJ, Forsyth MH, Cover TL, Song SY, Krishna U, Pietenpol JA. *Helicobacter pylori* strain-specific genotypes and modulation of the gastric epithelial cell cycle. *Cancer Res* 1999; 59:6124-31.
12. Toller IM, Neelsen KJ, Steger M, Hartung ML, Hottiger MO, Stucki M, Kalali B, Gerhard M, Sartori AA, Lopes M, et al. Carcinogenic bacterial pathogen *Helicobacter pylori* triggers DNA double-strand breaks and a DNA damage response in its host cells. *Proc Natl Acad Sci USA* 2011; 108:14944-9.
13. Koskela P, Anttila T, Bjørge T, Brunsvig A, Dillner J, Hakama M, Hakulinen T, Jellum E, Lehtinen M, Lenner P, et al. *Chlamydia trachomatis* infection as a risk factor for invasive cervical cancer. *Int J Cancer* 2000; 85:35-9.
14. Grieshaber SS, Grieshaber NA, Miller N, Hackstadt T. *Chlamydia trachomatis* causes centrosomal defects resulting in chromosomal segregation abnormalities. *Traffic* 2006; 7:940-9.
15. Johnson KA, Tan M, Sutterlin C. Centrosome abnormalities during a *Chlamydia trachomatis* infection are caused by dysregulation of the normal duplication pathway. *Cell Microbiol* 2009; 11:1064-73.
16. Knowlton AE, Brown HM, Richards TS, Andreolas LA, Patel RK, Grieshaber SS. *Chlamydia trachomatis* infection causes mitotic spindle pole defects independently from its effects on centrosome amplification. *Traffic* 2011; 12:854-66.
17. Brown HM, Knowlton AE, Grieshaber SS. Chlamydial infection induces host cytokinesis failure at abscission. *Cell Microbiol* 2012; 14:1554-67.
18. Sun HS, Wilde A, Harrison RE. *Chlamydia trachomatis* inclusions induce asymmetric cleavage furrow formation and ingression failure in host cells. *Mol Cell Biol* 2011; 31:5011-22.
19. Chumduri C, Gurumurthy RK, Zadora PK, Mi Y, Meyer TF. *Chlamydia* infection promotes host DNA damage and proliferation but impairs the DNA damage response. *Cell Host & Microbe* 2013; 13:746-58.

20. Hamon MA, Batsche E, Regnault B, Tham TN, Seveau S, Muchardt C, Cossart P. Histone modifications induced by a family of bacterial toxins. *Proc Natl Acad Sci USA* 2007; 104:13467-72.
21. Schmeck B, Beermann W, van Laak V, Zahlten J, Opitz B, Witzernath M, Hocke AC, Chakraborty T, Kracht M, Rosseau S, et al. Intracellular bacteria differentially regulated endothelial cytokine release by MAPK-dependent histone modification. *J Immunol* 2005; 175:2843-50.
22. Lebreton A, Lakisic G, Job V, Fritsch L, To NT, Camejo A, Mattei PJ, Regnault B, Nahori MA, Cabanes D, et al. A bacterial protein targets the BAHD1 chromatin complex to stimulate type III interferon response. *Science* 2011; 331:1319-21.
23. Sanger JM, Sanger JW. Insights into cell division using *Listeria monocytogenes* infections of PtK2 renal epithelial cells. *Cytoskeleton (Hoboken)* 2012; 69:992-9.
24. Cortez D. Caffeine inhibits checkpoint responses without inhibiting the ataxia-telangiectasia-mutated (ATM) and ATM- and Rad3-related (ATR) protein kinases. *J Biol Chem* 2003; 278:37139-45.
25. Joerges C, Kuntze I, Herzinger T. Induction of a caffeine-sensitive S-phase cell cycle checkpoint by psoralen plus ultraviolet A radiation. *Oncogene* 2003; 22:6119-28.
26. Chen BP, Chan DW, Kobayashi J, Burma S, Asaithamby A, Morotomi-Yano K, Botvinick E, Qin J, Chen DJ. Cell cycle dependence of DNA-dependent protein kinase phosphorylation in response to DNA double strand breaks. *J Biol Chem* 2005; 280:14709-15.
27. Park EJ, Chan DW, Park JH, Oettinger MA, Kwon J. DNA-PK is activated by nucleosomes and phosphorylates H2AX within the nucleosomes in an acetylation-dependent manner. *Nucleic Acids Res* 2003; 31:6819-27.
28. Wang H, Wang M, Wang H, Böcker W, Iliakis G. Complex H2AX phosphorylation patterns by multiple kinases including ATM and DNA-PK in human cells exposed to ionizing radiation and treated with kinase inhibitors. *J Cell Physiol* 2005; 202:492-502.

29. Donzelli M, Draetta GF. Regulating mammalian checkpoints through Cdc25 inactivation. *EMBO Rep* 2003; 4:671-7.
30. Sabatinos SA, Forsburg SL. Preserving the replication fork in response to nucleotide starvation: evading the replication fork collapse point. In: Stuart D, ed. *The Mechanisms of DNA Replication*, 2013.
31. Slaghuis J, Goetz M, Engelbrecht F, Goebel W. Inefficient replication of *Listeria innocua* in the cytosol of mammalian cells. *J Infect Dis* 2004; 189:393-401.
32. Poli J, Tsaponina O, Crabbe L, Keszthelyi A, Pantesco V, Chabes A, Lengronne A, Pasero P. dNTP pools determine fork progression and origin usage under replication stress. *EMBO J* 2012; 31:883-94.
33. Gomez-Diaz E, Jorda M, Peinado MA, Rivero A. Epigenetics of host-pathogen interactions: the road ahead and the road behind. *Plos Pathog* 2012; 8:e1003007.
34. Bierne H, Tham TN, Batsche E, Dumay A, Leguillou M, Kerneis-Golsteyn S, Regnault B, Seeler JS, Muchardt C, Feunteun J, et al. Human BAHD1 promotes heterochromatic gene silencing. *Proc Natl Acad Sci USA* 2009; 106:13826-31.
35. Cuevas-Ramos G, Petit CR, Marcq I, Boury M, Oswald E, Nougayrede JP. *Escherichia coli* induces DNA damage in vivo and triggers genomic instability in mammalian cells. *Proc Natl Acad Sci USA* 2010; 107:11537-42.
36. Guerra L, Guidi R, Frisan T. Do bacterial genotoxins contribute to chronic inflammation, genomic instability and tumor progression? *FEBS J* 2011; 278:4577-88.
37. Lara-Tejero M, Galan JE. A bacterial toxin that controls cell cycle progression as a deoxyribonuclease I-like protein. *Science* 2000; 290:354-7.
38. Wu M, Huang H, Zhang W, Kannan S, Weaver A, McKibben M, Herington D, Zeng H, Gao H. Host DNA repair proteins in response to *Pseudomonas aeruginosa* in lung epithelial cells and in mice. *Infect Immun* 2011; 79:75-87.
39. Vielfort K, Söderholm N, Weyler L, Vare D, Löfmark S, Aro H. *Neisseria gonorrhoeae* infection causes DNA damage and affects the expression of p21, p27, and p53 in non-tumor epithelial cells. *J Cell Sci* 2013; 126:339-47.

40. Bergounioux J, Elisee R, Prunier A-L, Donnadieu F, Sperandio B, Sansonetti P, Arbibe L. Calpain activation by the *Shigella flexneri* effector VirA regulates key steps in the formation and life of the bacterium's epithelial niche. *Cell Host & Microbe* 2012; 11:240-52.
41. Lam GY, Fattouh R, Muise AM, Grinstein S, Higgins DE, Brumell JH. Listeriolysin O suppresses phospholipase C-mediated activation of the microbicidal NADPH oxidase to promote *Listeria monocytogenes* infection. *Cell Host Microbe* 2011; 10:627-34.
42. Guerra L, Cortes-Bratti X, Guidi R, Frisan T. The biology of the cytolethal distending toxins. *Toxins (Basel)* 2011; 3:172-90.
43. Hardy J, Chu P, Contag CH. Foci of *Listeria monocytogenes* persist in the bone marrow. *Dis Model Mech* 2009; 2:39-46.
44. Rothman J, Paterson Y. Live-attenuated *Listeria*-based immunotherapy. *Expert Rev Vaccines* 2013; 12:493-504.
45. Brockstedt DG, Giedlin MA, Leong ML, Bahjat KS, Gao Y, Luckett W, Liu W, Cook DN, Portnoy DA, Dubensky TW, Jr. *Listeria*-based cancer vaccines that segregate immunogenicity from toxicity. *Proc Natl Acad Sci USA* 2004; 101:13832-7.
46. Yoshimura K, Jain A, Allen HE, Laird LS, Chia CY, Ravi S, Brockstedt DG, Giedlin MA, Bahjat KS, Leong ML, et al. Selective targeting of antitumor immune responses with engineered live-attenuated *Listeria monocytogenes*. *Cancer Res* 2006; 66:1096-104.
47. Reis O, Sousa S, Camejo A, Villiers V, Gouin E, Cossart P, Cabanes D. LapB, a novel *Listeria monocytogenes* LPXTG surface adhesin, required for entry into eukaryotic cells and virulence. *J Infect Dis* 2010; 202:551-62.
48. Edelstein A, Amodaj N, Hoover K, Vale R, Stuurman N. Computer control of microscopes using μ Manager. *Curr Protoc Mol Biol* 2010:14.20.1-14.20.17.

FIGURE LEGENDS

Figure 1. *Lm*-infected cells undergo consecutive rounds of division although with increased duration.

(A-C) Uninfected (NI) or *Lm*-infected (Inf, MOI 0.1) Caco-2 cells were followed by live-cell imaging for 72 h. Infection was confirmed by simultaneous acquisition of intracellular GFP signal and phase contrast images. (A) Time-lapse microscopy images from Movie S1 showing an infected cell dividing into two infected daughter cells. Top panel: phase contrast images; bottom panel: merged phase contrast and GFP signal images. Arrows show the dividing cell and resulting daughter cells. Specific cell cycle stages are depicted: interphase (0 min), nuclear envelope breakdown (80 min), (pro)metaphase (200 min), late anaphase (240 min), daughter cells in interphase (370 min). Partial time is indicated (0 corresponds to 29 h 40 min post-infection). Scale bar = 15 μ m. (B) Inset of Figure 1A showing *Lm* excluded from the mitotic spindle. Merged, phase contrast and GFP signal images are shown. (C) Quantification of the cell cycle duration in NI and Inf cells. The time elapsed between consecutive metaphase plates was determined in time-lapse images. Each dot represents a cell and the number of cells analyzed is indicated (n). Results are representative of five independent experiments. *** p-value < 0.001 (Student's t-test). (D) Cellular viability was examined 40 h after infection by PI incorporation and flow cytometry analysis. Results are means \pm SE from three independent experiments.

Figure 2. *Lm* infection induces alterations in the host cell cycle stage distribution.

(A, B) Caco-2 or Jeg-3 cells were left uninfected (NI) or infected (Inf, MOI 0.5 and 0.1, respectively) for 17 h. (A) Quantification of DNA histograms from PFA/ethanol-fixed cells (top panels). Inf GFP- corresponds to bystander cells lacking intracellular bacteria and Inf GFP+ to cells with intracellular bacteria. Representative DNA histograms are

shown (bottom panels). Results are means \pm SEM from at least three independent experiments. * indicate statistical comparisons to NI; # indicate statistical comparisons between Inf GFP- and Inf GFP+ populations. * and # p-value < 0.05, ** and ## p-value < 0.01, *** and ### p-value < 0.001 (one-way ANOVA). (B) Quantification of DNA histograms from ethanol-fixed cells (top panels) and representative histograms (bottom panels). Results are means \pm SEM from five independent experiments. * indicate statistical comparisons to NI. * p-value < 0.05, ** p-value < 0.01 (Student's t-test). (C) Quantification of cell cycle phase distribution of ethanol-fixed Caco-2 cells left NI or infected with increasing doses of *Lm* (MOI 0.1-1). Results are means \pm SEM from three independent experiments. * indicate statistical comparisons to NI. * p-value < 0.05, ** p-value < 0.01 (one-way ANOVA). (D) Quantification of DNA histograms from ethanol-fixed Caco-2 cells left NI or infected for 17 h with *Lm* (MOI 0.5) or *L. innocua*-InIA (*Li*-InIA, MOI 50). Results are means \pm SEM from five independent experiments. * indicate statistical comparisons to NI. * p-value < 0.05, *** p-value < 0.001 (one-way ANOVA). (E) Quantification of DNA histograms from PFA/ethanol-fixed Jeg-3 cells kept NI or infected with *Lm* Δ *inIA*, *Lm* Δ *inIB*, or *Lm* Δ *inIAB* (MOI 0.1, 17 h). Results are means \pm SEM from four independent experiments. * indicate statistical comparisons to NI; # indicate statistical comparisons between GFP- and GFP+ populations. * and # p-value < 0.05 (one-way ANOVA). (F) Quantification of DNA histograms from ethanol-fixed Caco-2 cells left NI or infected for 17 h with *Lm* (MOI 0.5) or *Lm* Δ *hly* (MOI 50). Results are means \pm SEM from three independent experiments. * indicate statistical comparisons to NI; # indicate statistical comparisons between *Lm* and *Lm* Δ *hly*. * and # p-value < 0.05, ** p-value < 0.01 (one-way ANOVA).

Figure 3. *Lm* infection induces a delayed S-phase progression in Caco-2 cells.

(A, B) Caco-2 cells synchronized at G1/S-phase transition by double thymidine block were released from the cell cycle arrest (0 h), left uninfected (NI) or infected with *Lm* (Inf, MOI 20) and DNA histograms were generated from ethanol-fixed cells 5 h post-

infection. (A) Representative DNA histograms of two independent experiments. (B) Analysis of split S-phase statistics (S1, S2, S3 and S4, ranging from lower to higher DNA content) representative of two independent experiments. (C-E) NI or *Lm*-infected (Inf, 18 h) Caco-2 cells were allowed to incorporate EdU during the last 2h before analysis. (C) Representative flow cytometry density plots showing the discrimination and percentage of S-phase cells (EdU+ population). (D) Quantification of the percentage of S-phase (EdU+) cells. Results are means \pm SEM from three independent experiments. * p-value < 0.05 (Student's t-test). (E) Quantification of the mean fluorescence intensity (EdU+ MFI). Results are means \pm SEM from three independent experiments. Values are given relative to NI cells, arbitrarily fixed at 100. * p-value < 0.05 (one-sample t-test). (F, G) After EdU incorporation, NI or *Lm*-infected Caco-2 cells were allowed to progress for 5h, before analysis. (F) Representative flow cytometry contour plots showing the cell cycle progression of EdU-labeled cells 5 h after EdU washout. Red arrow shows EdU+ G1/G0 cells. (G) Quantification of the percentage of EdU+ cells in S and G1/G0 phases, 5 h after EdU pulse. Results are means \pm SEM from three independent experiments. * p-value < 0.05 (Student's t-test).

Figure 4. *Lm* infection induces DNA strand breaks in host cells.

(A, B, E) Caco-2 cells were left uninfected (NI) or infected with *Lm* (Inf, MOI 0.5). Etoposide-treated (Etop) and γ -irradiated (IR) cells were used as positive controls. (A) DNA strand breaks measured by single-cell gel electrophoresis (SCGE). Left panels: representative images of comets with respective Comet Assay IV software screenshots for each condition. Right panel: quantification of comet tail intensities. Each dot represents a single comet. The number of comets analyzed per condition is indicated (n). Data are representative of three independent experiments. * p-value < 0.05, *** p-value < 0.001 (one-way ANOVA). (B) DNA integrity assessed by pulse field gel electrophoresis (PFGE). Bands corresponding to intact and fragmented genomic DNA are indicated (left panel) and their relative intensity was quantified (right panel). Data

are representative of three independent experiments. (C) Caco-2 cells were left NI or infected with *Lm* (MOI 0.5) or *Lm* Δ *hly* (MOI 10) and the DSB marker γ H2A.X was evaluated by immunoblot. Levels of γ H2A.X were normalized to total H2A.X and the value for infected cells was expressed relative to the ratio of NI cells, arbitrarily fixed to 100. Graph shows means \pm SE from three independent experiments. * p-value < 0.05 (one-sample t-test). (D) Caco-2 cells were left NI or infected with increasing doses of *Lm* (MOI 0.1-1, 20 h) and the DSB marker γ H2A.X was quantified by immunoblot. GAPDH was used as loading control. (E) Assessment of γ H2A.X levels by immunofluorescence. Merged images show γ H2A.X foci in red and DAPI-stained nuclei in blue (left panel). Scale bar = 20 μ m. Graph shows means \pm SEM from four independent experiments. Approximately 500 nuclei were analyzed per condition. Integrated pixel density of γ H2A.X foci was normalized to the total number of nuclei. Infected sample values were expressed relative to the NI sample value arbitrarily fixed to 100. * p-value < 0.05 (Student's t-test).

Figure 5. DNA damage checkpoint function is required to favor *Lm* infection.

(A-F) Caco-2 cells were left uninfected (NI) or infected with *Lm* (Inf, MOI 0.5, 20 h), in the presence or absence of 2 mM caffeine, or subjected to increasing concentrations of etoposide (0-10 μ M). γ -irradiated cells (IR) were used as controls. (A) Quantification of DNA histograms from ethanol-fixed cells (top panel). Results are means \pm SEM from four independent experiments. Representative histograms are shown (bottom panels). * indicate statistical comparisons to NI, in the presence or absence of caffeine; # indicate statistical comparisons between groups, in presence and absence of caffeine. * and # p-value < 0.05, ## p-value < 0.01, *** and ### p-value < 0.001 (one-way ANOVA). (B) Quantification of the cell cycle duration of NI and Inf cells, in the presence or absence of caffeine. The time elapsed between consecutive metaphase plates was measured in time-lapse images. The number of cells analyzed is indicated (n). Results are representative of two independent experiments. * p-value < 0.05, *** p-value <

0.001 (one-way ANOVA). (C-F) Caffeine and etoposide interfere with *Lm* infectious potential in opposing manners. (C) Representative flow cytometry density plots showing the percentage of infected cells (GFP+ population) and their mean GFP fluorescence intensity (dotted line), in the presence or absence of caffeine. (D) Quantification of the percentage of infected cells (left panel), mean GFP fluorescence intensity (GFP+ MFI, middle panel) and intracellular bacteria (right panel), in the presence or absence of caffeine. Graphs show means \pm SEM from three independent experiments. Values are expressed relative to the infection without caffeine, arbitrarily fixed to 100. * p-value < 0.05, ** p-value < 0.01 (one-sample t-test). (E) Representative flow cytometry density plots showing the percentage of infected cells (GFP+ population) and their mean GFP fluorescence intensity (dotted line), in the presence or absence of 10 μ M etoposide. (F) Graphs show means \pm SEM of the percentage of infected cells (left panel) and mean GFP fluorescence intensity (GFP+ MFI, right panel), in the absence or presence of 1 and 10 μ M etoposide, from three independent experiments. Values are expressed relative to the infection in the absence of etoposide, arbitrarily fixed to 100. ** p-value < 0.01 (one-sample t-test).

Figure 6. *Lm*-induced alterations of the host cell cycle profile are dependent on DNA-PK.

(A-C) Expression of ATM, ATR and DNA-PK was silenced in Caco-2 cells by transfecting simultaneously ATM and ATR (siATM/ATR) or DNA-PK (siDNA-PK) specific siRNAs. Control cells were transfected with non-targeting siRNAs (siCtr). Cells were left uninfected (NI) or infected with *Lm* (Inf, MOI 0.5, 20 h). (A) Quantification of DNA histograms from ethanol-fixed cells. Results are means \pm SEM from at least three independent experiments. * indicate statistical comparisons to NI siCtr; # indicate statistical comparisons between control and targeting siRNAs. * and # p-value < 0.05, ## p-value < 0.01, *** p-value < 0.001 (one-way ANOVA). (B) Quantification of the percentage of infected cells (GFP+) and the mean GFP fluorescence intensity (GFP+

MFI) by flow cytometry. Graphs show means \pm SEM from at least three independent experiments. Values are given relative to the infection of siCtr cells, arbitrarily fixed at 100. ** p-value < 0.01 (one-sample t-test). (C) Evaluation of ATM, ATR and DNA-PK expression levels by immunoblot. Top panels show representative immunoblots. Bottom panels show quantifications of GAPDH-normalized ATM, ATR and DNA-PK expression levels. Expression levels in silenced conditions are given relative to siCtr, arbitrarily fixed to 100. Graph shows means \pm SEM from two (siATM/ATR) or three (siDNA-PK) independent experiments. * p-value < 0.05 (one-sample t-test).

Figure 7. DNA-PK and CDC25A are mediators of the DNA damage/repair signaling cascade elicited by *Lm* infection, both *in vitro* and *in vivo*.

(A) Uninfected (NI)/untreated (NT) Caco-2 cells were exposed to increasing MOIs or etoposide doses for 20 h and phosphorylation levels of DNA-PK (p-DNA-PK), H2A.X (γ H2A.X) and CDC25A (p-CDC25A) were assessed by immunoblot. GAPDH was used as loading control. Representative immunoblots are shown (top panels). Quantification graphs (bottom panels) show means \pm SEM of three independent experiments. Values for infected/treated conditions were expressed relative to NI or NT conditions, arbitrarily fixed to 100. * p-value < 0.05 (one-sample t-test). (B, C) Analysis of γ H2A.X and p-CDC25A levels during *Lm* infection *in vivo*. BALB/c mice were left uninfected (NI) or infected (Inf) for 1 (B) or 3 days (C) with *Lm* and the levels of γ H2A.X and p-CDC25A were evaluated by immunoblot on total extracts from mouse spleen cells. Two independent experiments were performed using two mice per condition (#1, #2). Immunoblot images (top panels) and quantifications of GAPDH-normalized phosphorylation levels (bottom panels) are shown.

SUPPLEMENTAL INFORMATION

Experimental Procedures

Bacterial strains, cell lines and growth conditions

Listeria monocytogenes EGDe-cGFP¹ (designated as *Lm*), isogenic *hly*-, *inlA*-, *inlB*- and *inlAB*-defective mutants expressing GFP (this study, designated as *LmΔhly*, *LmΔinlA*, *LmΔinlB*, and *LmΔinlAB*, respectively) and *Listeria innocua* expressing InlA² (designated *Li-InlA*) were grown in Brain Heart Infusion (BHI, Difco Laboratories) broth supplemented with 7 μg/ml chloramphenicol, at 37°C under aerobic conditions with agitation. Human colorectal adenocarcinoma cell line Caco-2 (ATCC HTB-37) was propagated in complete growth medium [Eagle's Minimum Essential Medium (EMEM), 20% (v/v) fetal bovine serum (FBS), 1 mM sodium pyruvate, 0.1 mM non-essential amino acids], at 37°C in a 7% CO₂ humidified atmosphere. Human choriocarcinoma cell line Jeg-3 (ATCC HTB-36) was cultured in similar conditions except that the medium was supplemented with 10% FBS. Cell culture medium and supplements were purchased from Lonza. Whenever stated, cells were treated with 0.1, 1, 10, 20, or 40 μM etoposide (Sigma) for 17-20 h, or exposed to γ-rays (5 Gy) using a ¹³⁷Cs source (Gammacell 1000 irradiator, Nordion) to induce DNA strand breaks.

Infection of synchronized cells

Caco-2 cell suspensions were seeded at 4x10⁵ cells per 60-mm dish and synchronized at the G1/S-phase boundary by a double thymidine block (2 mM thymidine for 18 h, released for 8 h, and a second arrest with 2 mM thymidine for 18 h). Cells were released from G1/S block, incubated for 1 h with *Lm* suspension at MOI 20 and allowed to progress into S-phase for 4 h in complete medium supplemented with 50 μg/ml gentamicin. Cells were washed, harvested by trypsinization and processed for flow cytometry analyses.

Single-cell gel electrophoresis (SCGE or Comet assay)

Eukaryotic cell DNA damage was measured by alkaline single-cell gel electrophoresis according to methods previously described^{3,3}. Approximately 10^4 cells harvested by trypsinization were suspended in 0.6% low melting point agarose prepared in PBS. The mixture was dispensed onto glass microscope slides previously coated with 1% normal melting point agarose, and allowed to set on ice under a coverslip. Coverslips were removed and slides kept overnight in ice-cold lysis buffer [10 mM Tris, 100 mM disodium EDTA, 2.5 M NaCl, pH 10, with 1% Triton X-100 (v/v) freshly added], and washed in ice-cold distilled water. In a horizontal electrophoresis tank, slides were kept submerged in ice-cold alkaline electrophoresis solution (300 mM NaOH, 1 mM disodium EDTA) for 20 min. Electrophoresis was performed for 1 h (0.66 V/cm, 300 mA) at 4°C. Slides were neutralized with PBS for 20 min and washed with double-distilled water, before drying at 37°C. All procedures were carried out under subdued light to minimize background DNA damage. Slides were rehydrated in distilled water, stained with 2.5 µg/ml propidium iodide (PI) for 20 min, washed for 30 min and allowed to dry at 37°C. Comets were visualized under an Axioskop fluorescence microscope (Zeiss) at 200x magnification, and images were captured by an AxioCamMR camera (Zeiss). Approximately 150 cells were analyzed per sample, 50 per triplicate slide. Comet Assay IV™ software (Perceptive Instruments) was used to score the percentage of DNA in the comet tail (% tail intensity). The intensity of the tail relative to the head reflects the extent of DNA breaks.⁴

Pulse-field gel electrophoresis (PFGE)

Detection of DNA double strand breaks (DSBs) by PFGE was performed according to previously described methods^{5,6} with modifications. Trypsinized cells were washed and 0.75% agarose plugs of 5×10^5 cells were prepared with CHEF Mammalian Genomic DNA Plug Kit following the manufacturer instructions (BioRad Laboratories). Plugs

were incubated overnight with proteinase K at 50 °C, without agitation, washed and submitted to electrophoresis for 21 h at 14 °C in 0.9% (w/v) SeaKem Gold Agarose (Lonza) prepared in 0.5x Tris/borate/EDTA (TBE, BioRad Laboratories) using a CHEF DR III apparatus (BioRad Laboratories) with three consecutively executing blocks of running conditions (block 1: 9 h, included angle 120°, switch time 30 to 18 s, 5.5 V/cm; block 2: 6 h, included angle 117°, switch time 18 to 9 s, 4.5 V/cm; and block 3: 6 h, included angle 112°, switch time 9 to 5 s, 4.0 V/cm). Under these conditions, mammalian genomic DNA fragments of lower molecular weight enter the gel, while high molecular weight DNA remains in the well. Gels were stained with ethidium bromide and images acquired with a Molecular Imager Gel Doc™ XR+ System (BioRad Laboratories).

Immunoblot analyses

Cells were washed with ice-cold PBS and resuspended in 1x SDS-PAGE loading buffer (3% glycerol, 5% mercaptoethanol, 2% SDS, 0.1% blue bromophenol in 1 M Tris-HCl pH 6.8). Lysates were incubated with benzonase nuclease (Sigma) to shear DNA and heated at 95°C during 5 min. Samples were resolved in a 4%15% Mini-Protean®TGX™ PreCast Gel (BioRad Laboratories) and transferred onto a 0.2 µm nitrocellulose membrane (Trans-Blot®Turbo™ Transfer Pack, BioRad Laboratories) during 15 min at 1.3 A in a TransBlot®Turbo System (BioRad Laboratories). After blocking with 5% non-fat dry milk or 4% BSA in Buffer A (150 mM NaCl, 20 mM Tris-HCl pH 7.4 and 0.1% Triton X-100), at least 1 h at room temperature, membranes were immunoblotted overnight at 4°C with primary antibodies anti-pSer139 H2A.X (clone JBW301, Millipore), anti-pSer2056 DNA-PK (ab18192; Abcam), anti-pSer76 CDC25A (ab75743; Abcam), anti-ATM (sc-23921), anti-histone H2A.X (sc-54606), anti-ATR N-19 (sc-1887), anti-DNA-PK (sc-9051), anti-CDC25A (sc-7389) and anti-GAPDH (sc-32233) from Santa Cruz Biotechnology. Membranes were washed three times and incubated during 1 h at room temperature with anti-mouse and anti-rabbit (PARIS Biotech) or

anti-goat (Santa Cruz Biotechnology) horseradish peroxidase-conjugated secondary antibodies. After washing, antibody signal was revealed by chemiluminescent autoradiography using Pierce[®] ECL Western Blotting Substrate (Thermo Scientific). Band intensity was quantified using Image Lab 3.0 software (BioRad Laboratories).

Immunofluorescence analyses

Caco-2 cells grown on top of coverslips were infected or left uninfected, fixed with 3% PFA (20 min), quenched with 50 mM NH₄Cl (30 min) and permeabilized with 0.1% Triton X-100 (5 min). To quantify cells infected by *Li-InlA*, cells were incubated with rabbit anti-*L. innocua* antibodies R6⁷ diluted 1:500 in blocking solution (1% BSA and 20% FBS in PBS), followed by incubation with AlexaFluor488-conjugated anti-rabbit antibody (Invitrogen) diluted 1:150; phalloidin-TRITC (Sigma) diluted 1:500 and 2 ng/ml DAPI (Sigma). Coverslips were mounted with Mowiol mounting medium (Kuraray Specialties Europe GmbH). For quantification of *Lm*-infected cells, cells were only incubated with phalloidin-TRITC and DAPI in blocking solution. Quantification of infected cells was performed by visual inspection under an Olympus BX53 microscope. For γ H2A.X quantification, cells were incubated with mouse anti-pSer139 histone H2A.X (Millipore) diluted 1:500 in blocking solution, followed by incubation with Cy3-conjugated anti-mouse antibody (Jackson ImmunoResearch) diluted 1:150 and DAPI. Images were acquired with a 20x (0.17NA) objective and Image J software⁸ was used for image quantification. Analyses were performed by quantifying the integrated density of pixels corresponding to γ H2A.X foci and normalizing the resulting values to the total number of nuclei.

Transfection of siRNA duplexes

Caco-2 cells were transfected using the Amaxa Cell Line Nucleofector Kit T as indicated by the manufacturer (Lonza). ATM siRNA (sc-29761), ATR siRNA (sc-29763), DNA-PK siRNA (sc-35200) as well as siRNA control (sc-44232) were

purchased from Santa Cruz Biotechnology. Cells were left uninfected or infected 72 h after transfection and analyzed 18-20 h later.

Flow cytometry analyses

To distinguish cells infected with *Li*-InIA (*Li*-APC+) from the bystander population (*Li*-APC-), samples fixed with PFA-ethanol were incubated with rabbit anti-*L. innocua* R6⁷ diluted in 1% FBS in PBS, followed by incubation with Cy5-conjugated anti-rabbit antibody (Jackson Immuno Research). Cells were then analyzed on a APC-A/FSC-A plot followed by an analysis on the PE-A channel, which allows the generation of independent DNA histograms for each population.

Mice experiments

Infections were performed as previously described.⁹ Six-week-old specific pathogen-free female BALB/c mice (Charles River) were injected intravenously with a sub-lethal bacterial inoculum, 10⁴ CFUs and spleens were recovered (two animals per condition) 1 or 3 days after infection. Spleen cells were isolated by passing through a cell strainer and washing them in PBS supplemented with 2% FBS. Cell viability was evaluated by flow cytometry after PI incorporation as described before. The cell suspension was centrifuged at 1000 g for 5 min and the pellet was resuspended in 1x SDS-PAGE loading buffer for immunoblot analysis, as described above.

Ethics Statement

This study was carried out in accordance with European and Portuguese legislation for the use of animals for scientific purposes (Directive 86/609/EEC; Decreto-Lei 129/92; Portaria 1005/92). The work was approved by Direcção Geral de Veterinária, the Portuguese authority for animal protection (ref. ERA-PTG/0003/2010).

Preparation of *Lm* genomic DNA plugs for PFGE

Plugs containing only *Lm* (10^6 - 10^8 bacteria per plug) were prepared using the same protocol described in Experimental Procedures.

In vitro* growth of *Lm

Lm growth curves were obtained in BHI broth at 37°C, under aerobic conditions, with agitation, in the presence or absence of 2 mM caffeine. The OD₆₀₀ values were recorded every 45 min until the stationary phase.

References

1. Balestrino D, Hamon MA, Dortet L, Nahori M-A, Pizarro-Cerda J, Alignani D, Dussurget O, Cossart P, Toledo-Arana A. Single-cell techniques using chromosomally tagged fluorescent bacteria to study *Listeria monocytogenes* infection processes. *Appl Environ Microbiol* 2010; 76:3625-36.
2. Lecuit M, Ohayon H, Braun L, Mengaud J, Cossart P. Internalin of *Listeria monocytogenes* with an intact leucine-rich repeat region is sufficient to promote internalization. *Infect Immun* 1997; 65:5309-19.
3. Duarte TL, Almeida GM, Jones GD. Investigation of the role of extracellular H₂O₂ and transition metal ions in the genotoxic action of ascorbic acid in cell culture models. *Toxicol Lett* 2007; 170:57-65.
4. Collins AR. The comet assay for DNA damage and repair - Principles, applications, and limitations. *Mol Biotechnol* 2004; 26:249-61.
5. Hanada K, Budzowska M, Davies SL, van Drunen E, Onizawa H, Beverloo HB, Maas A, Essers J, Hickson ID, Kanaar R. The structure-specific endonuclease Mus81 contributes to replication restart by generating double-strand DNA breaks. *Nat Struct Mol Biol* 2007; 14:1096-104.

6. Toller IM, Neelsen KJ, Steger M, Hartung ML, Hottiger MO, Stucki M, Kalali B, Gerhard M, Sartori AA, Lopes M, et al. Carcinogenic bacterial pathogen *Helicobacter pylori* triggers DNA double-strand breaks and a DNA damage response in its host cells. Proc Natl Acad Sci USA 2011; 108:14944-9.
7. Dramsi S, Lévi S, Triller A, Cossart P. Entry of *Listeria monocytogenes* into neurons occurs by cell-to-cell spread: an in vitro study. Infect Immun 1998; 66:4461-8.
8. Schneider CA, Rasband WS, Eliceiri KW. NIH Image to ImageJ: 25 years of image analysis. Nat Methods 2012; 9:671-5.
9. Cabanes D, Lecuit M, Cossart P. Animal models of *Listeria* infection. Curr Protoc Microbiol 2008; Chapter 9:Unit9B 1.

Figure Legends

Movie S1 (related to Figure 1). *Lm*-infected cells undergo cell division originating infected daughter cells.

Caco-2 cells were infected (Inf, MOI 0.1) and followed by live-cell imaging during 72 h. *Lm* infection was confirmed by simultaneous acquisition of GFP signal and phase contrast images. Scale bar = 50 μ m. Frame rate: 15 frame per second (MP4).

Movie S2 (related to Figure 1). *Lm*-infected cell undergoing consecutive rounds of division.

Caco-2 cells were infected (Inf, MOI 0.1) and followed by live-cell imaging during 72 h. *Lm* infection was confirmed by simultaneous acquisition of GFP signal and phase contrast images. Scale bar = 25 μ m. Frame rate: 15 frame per second (MP4).

Figure S1 (related to Figure 2). *Lm* infections of Caco-2 cells do not interfere with cell viability.

(A) Caco-2 cells were left uninfected (NI) or infected with *Lm* (Inf, MOI 0.5, 17 h). Representative flow cytometric PE-A/PerCP-Cy5-A density plots are shown. Viability was examined in unfixed cells incubated in the presence of propidium iodide. (B) After exclusion of dead cells, the percentage of infected cells (GFP+ population) was determined on a GFP-A/PE-A plot. Graphs show means \pm SE from five independent experiments (same as in Figure 2B, left panel).

Figure S2 (related to Figure 2). *Lm*-induced alterations in the host cell cycle are detected at low percentages of infection.

Caco-2 cells were left uninfected (NI) or infected with *Lm* (Inf, MOI 0.5, 17 h). Similar to Figure 2B (left panel), except that average infected cells is 33%. Results are means \pm SE from five independent experiments. ** p-value < 0.01, *** p-value < 0.001 by Student's t-test.

Figure S3 (related to Figure 2). *Li*-InIA infection does not interfere with the host cell cycle.

Quantification of flow cytometric DNA histograms from Caco-2 cells left uninfected (NI) or infected with *Li*-InIA (MOI 50, 17 h) and fixed with PFA-ethanol. Intracellular *Li*-InIA bacteria were labeled with antibodies raised against *Li* allowing the discrimination of bystander cells (*Li*-APC-) and *Li*-InIA-infected cells (*Li*-APC+) populations. Results are means \pm SE from three independent experiments.

Figure S4 (related to Figure 4). Fragmented DNA detected by PFGE from *Lm*-infected cells is not from bacterial origin.

Plugs containing different quantities of *Lm* (*Lm*-only) were prepared, and after electrophoresis, gel images were acquired. Plugs containing uninfected (NI) and infected (Inf) Caco-2 cells were used as controls.

Figure S5 (related to Figure 5). *In vitro* growth of *Lm* is not affected by caffeine.

Growth curve of *Lm* in BHI broth under aerobic conditions at 37°C with agitation, in the absence (CTR) or presence of 2 mM caffeine. Data are representative of four independent experiments.

Figure S6 (related to Figure 7). *Lm* infection does not interfere with mouse spleen

cell viability. Viability of cells isolated from infected mice spleens was evaluated through flow cytometry by determining PI exclusion. Two mice were evaluated per condition, 1 day and 3 days after intravenous infection.

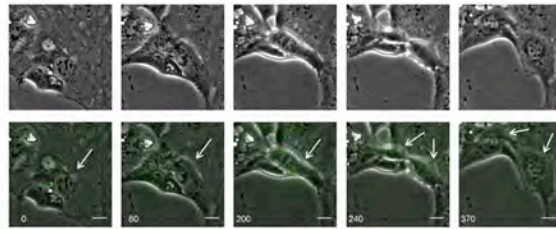
Tables

Table S1 (relative to Figure 4B). Relative intensity of fragmented DNA bands obtained for three independent PFGE experiments.

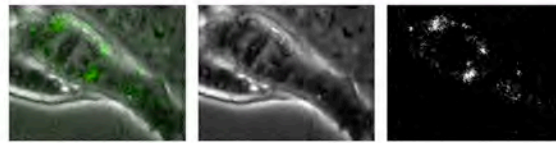
	#1	#2	#3
NI	100	100	100
Inf	148	185	113
Etop	152	246	144
IR	136	194	n.a.

n.a.: not applicable

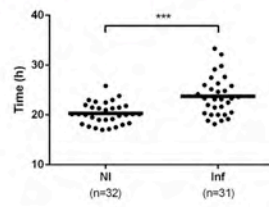
A



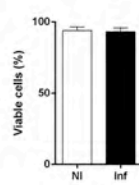
B

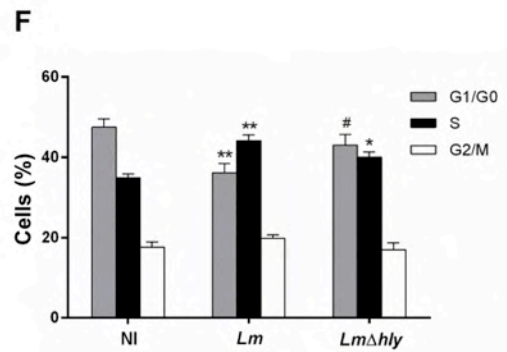
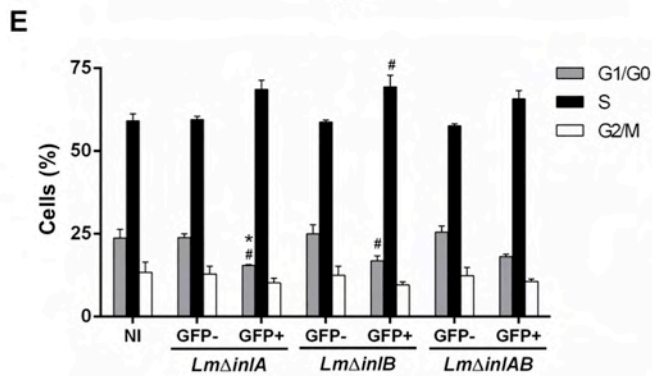
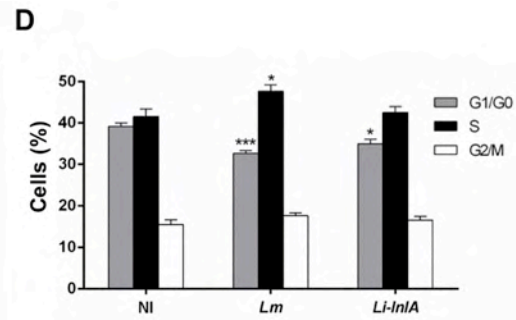
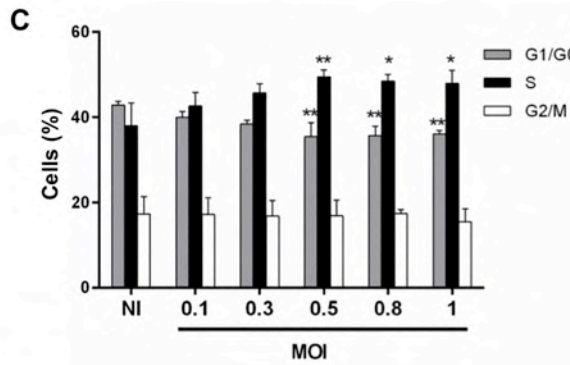
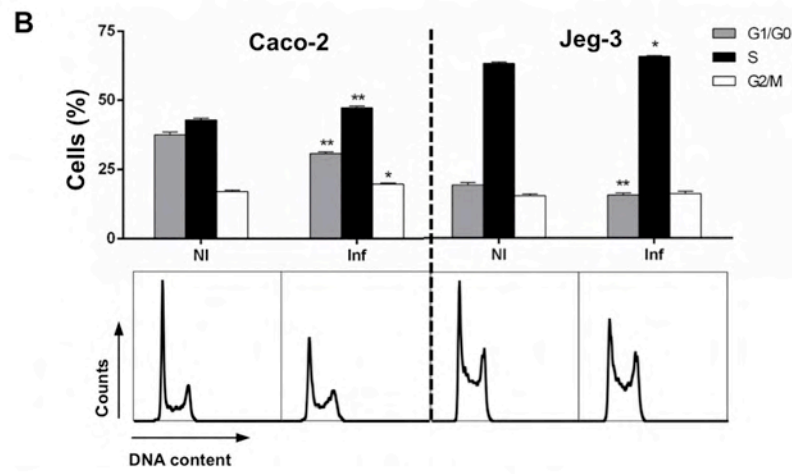
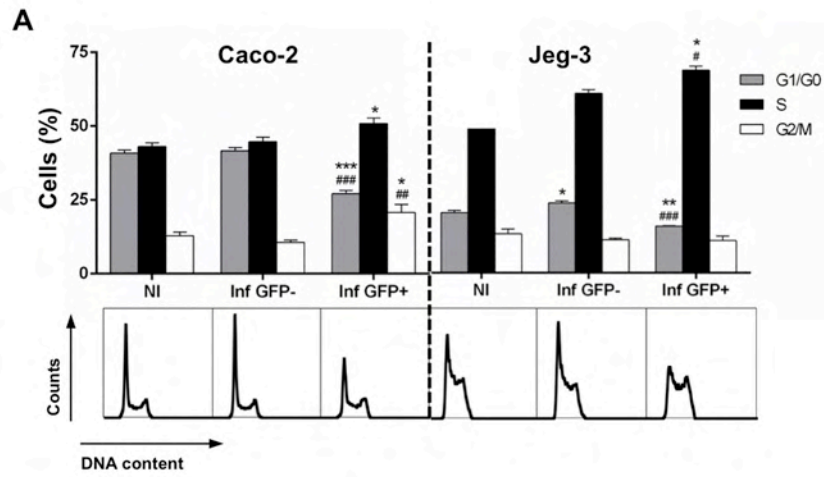


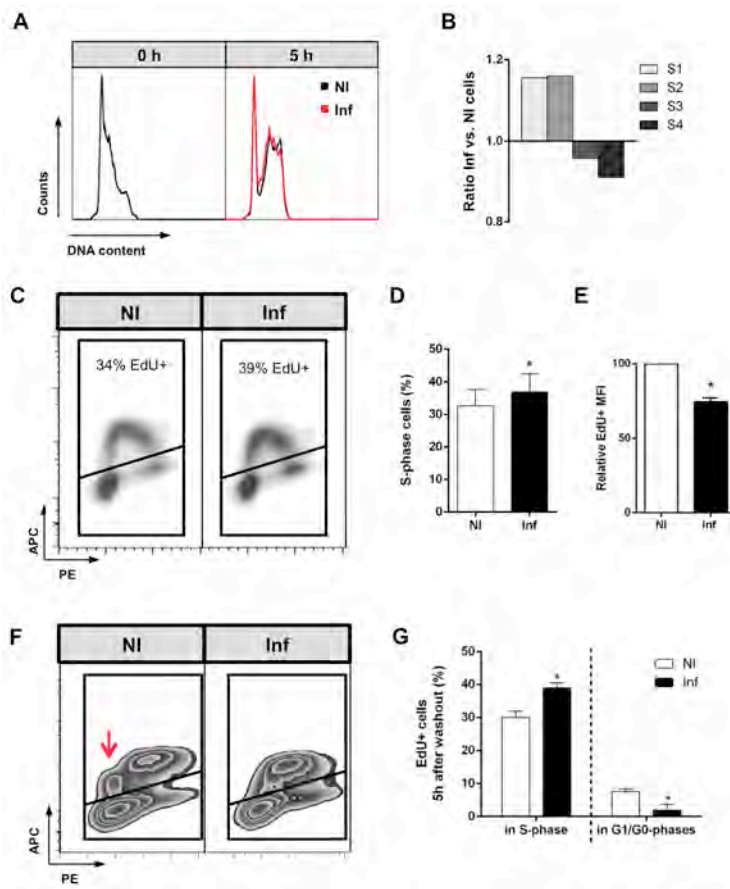
C

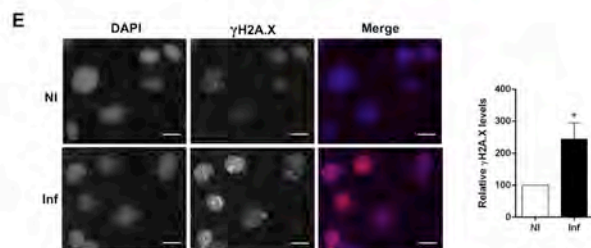
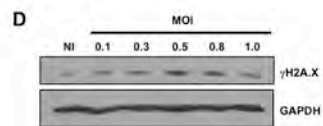
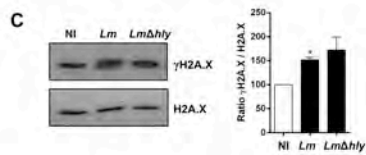
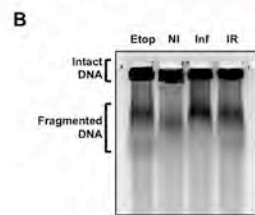
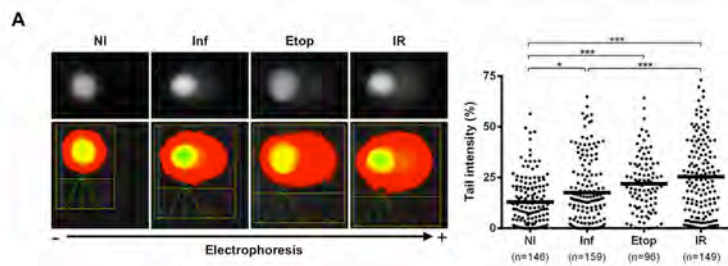


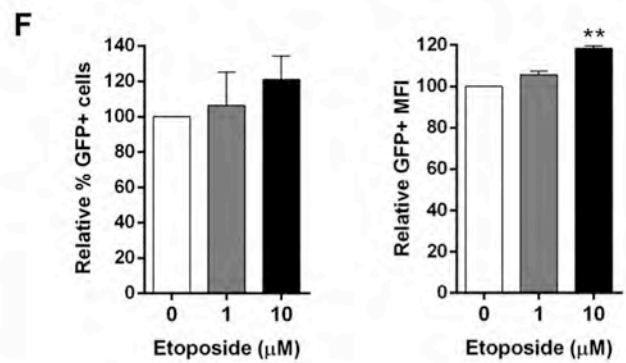
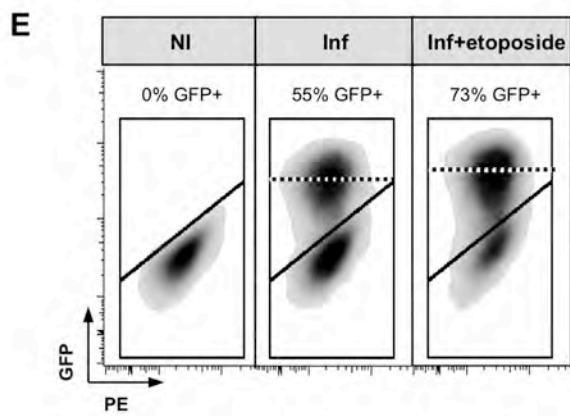
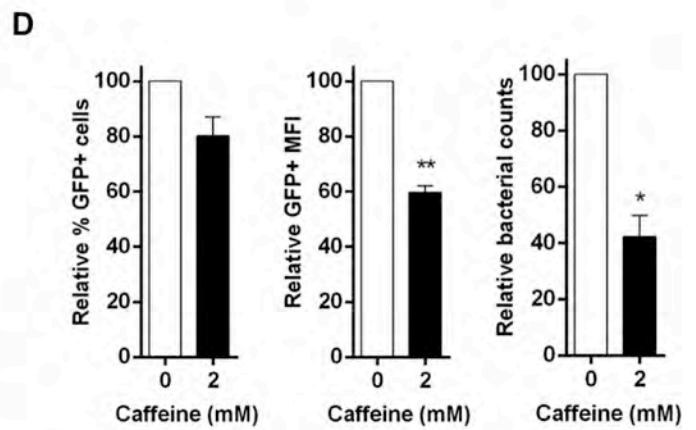
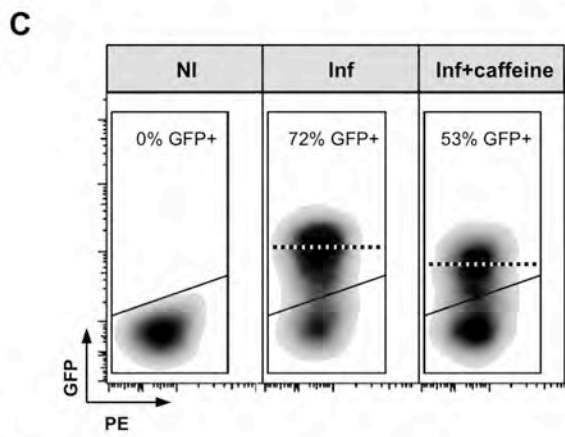
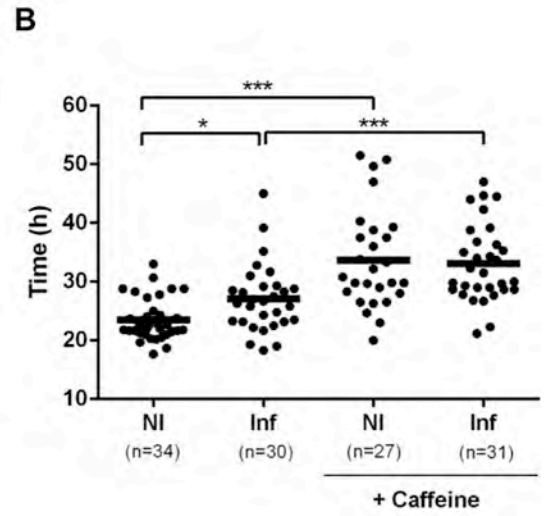
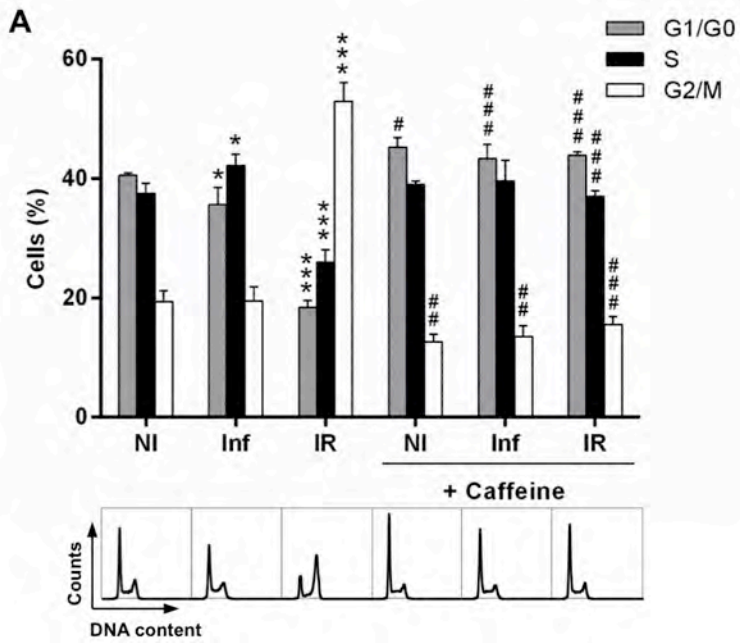
D

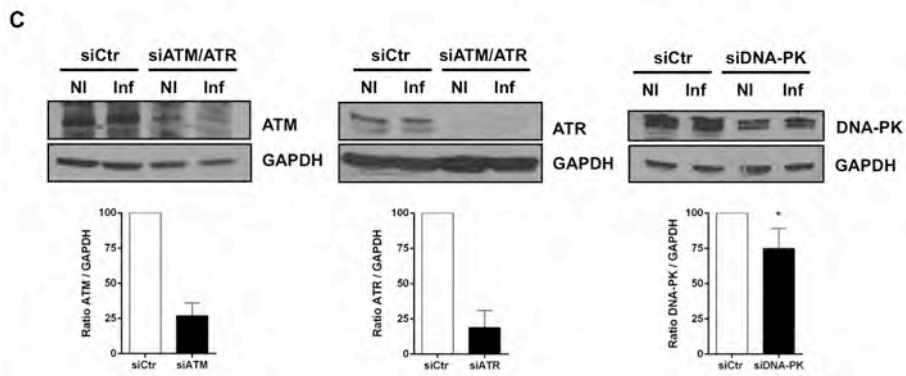
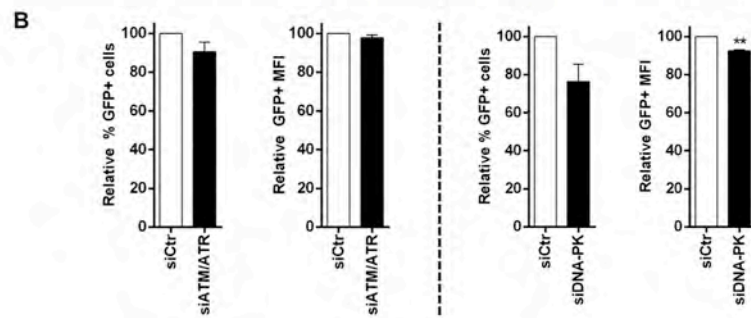
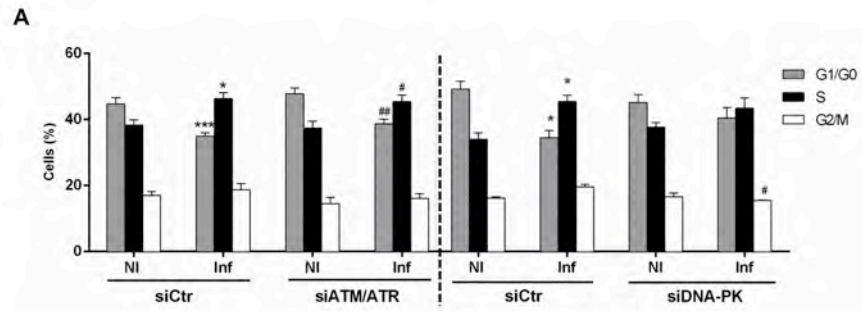




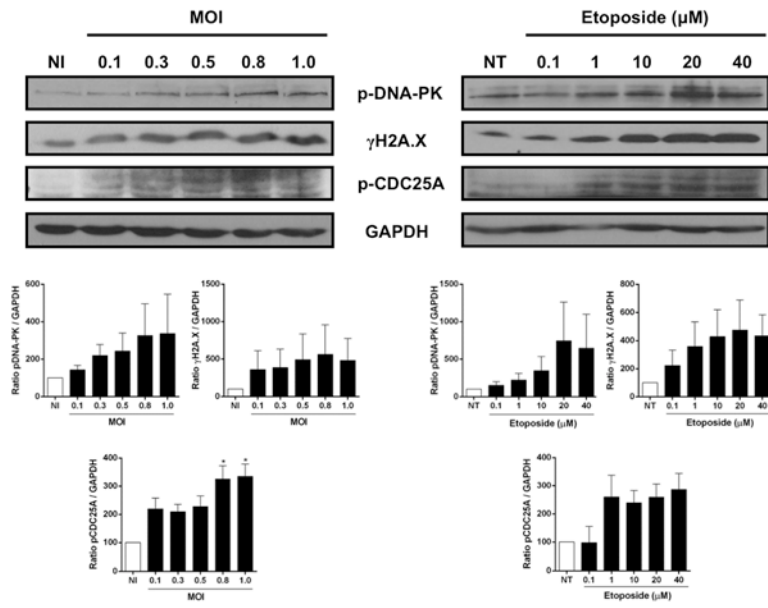




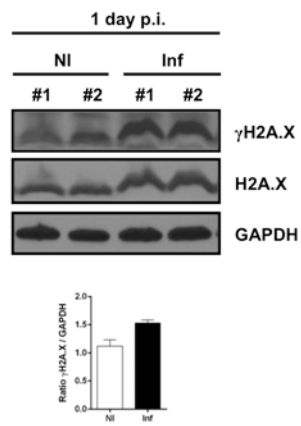




A



B



C

